

BWRVIP

BWR Vessel & Internals Project _____ 2000-163

June 14, 2000

Document Control Desk
U. S. Nuclear Regulatory Commission
11555 Rockville Pike
Rockville, MD 20852

Attention: C. E. Carpenter

Subject: Project 704 - Transmittal of "BWR Vessel and Internals Project, Weldability of Irradiated LWR Structural Components (BWRVIP-45NP)," EPRI Report TR-108707NP, May 2000.

Reference: Letter from C. Terry to C. E. Carpenter, October 27, 1997: Transmittal of "BWR Vessel and Internals Project, Weldability of Irradiated LWR Structural Components (BWRVIP-45)," EPRI Report TR-108707, September 1997.

Enclosed are two (2) copies of the subject report "BWR Vessel and Internals Project, Weldability of Irradiated LWR Structural Components (BWRVIP-45)," EPRI Report TR-108707, September 1997. This is the non-proprietary version of the document submitted to the NRC by the letter referenced above.

If you have any questions on this subject please call Steve Lewis of Entergy, BWRVIP Assessment Committee Chairman, at (601) 368-5444.

Sincerely,



Carl Terry
Niagara Mohawk Power Company
Chairman, BWR Vessel and Internals Project

Enclosure

1/2

BWR Vessel and Internals Project Weldability of Irradiated LWR Structural Components (BWRVIP-45NP)

NON-PROPRIETARY INFORMATION

NOTICE: This report contains the non-proprietary information that is included in the proprietary version of this report. The proprietary version of this report contains proprietary information that is the intellectual property of BWRVIP utility members and EPRI. Accordingly, the proprietary report is available only under license from EPRI and may not be reproduced or disclosed, wholly or in part, by any Licensee to any other person or organization.

BWR Vessel and Internals Project

Weldability of Irradiated LWR Structural Components
(BWRVIP-45NP)

Boiling Water Reactor Vessel and Internals Project (BWRVIP), formed in June 1994, is an association of utilities focused exclusively on BWR vessel and internals issues. This report describes work performed to determine the effects of irradiation on the weldability of reactor internals.

INTEREST CATEGORIES

Piping, reactor vessel
and internals
Licensing and safety
assessment

KEYWORDS

Boiling water reactor
Irradiation
Stress corrosion cracking
Vessel and internals
Weldability

BACKGROUND A number of BWRs have experienced cracking in various internal components due to intergranular stress corrosion cracking. In some cases, the preferred method for repairing these components is underwater welding. However, experience has shown that if the base metal is highly irradiated inferior welds can result. At high fluences, helium is generated in the material due to transmutation of boron and nickel through neutron absorption. During the welding process, this helium is released and forms bubbles which cause cracks and inclusions in the weld.

OBJECTIVES To determine the fluence threshold at which welding becomes problematic and to develop a map of a typical BWR showing which regions are weldable and which are not.

APPROACH The project team first conducted a literature search to determine the threshold level of helium at which successful welds could be made. Next, the team performed a neutron transport calculation to establish the thermal neutron flux and helium generation rates at all points in a typical BWR. Finally, the results of the above tasks were combined to show calculated helium content at all points in the reactor at 1, 15 and 30 full power years.

RESULTS

**Content Deleted -
EPRI Proprietary Information**

EPRI PERSPECTIVE These results are useful in providing general guidance on the acceptability of performing weld repairs on reactor internals. However, it must be noted that the helium content at which welding becomes problematic is not precisely defined. It appears to be dependent on a number of factors which are not well quantified. In addition, methods for calculating the thermal neutron fluence (and the helium generation) in the ex-core region are not as precise as for the in-core region.

Improvements in the threshold definition and in the flux calculations would be useful.

PROJECT

WOB501

EPRI Project Manager: Warren Bilanin

Business Group: Nuclear Power Group

Contractor: ORNL

For ordering information about this report, call the EPRI Program Manager at (650) 855-2340.

For membership information, call (650) 855-2514.

BWR Vessel and Internals Project

Weldability of Irradiated LWR Structural Components (BWRVIP-45NP)

TR-108707NP
Research Project 501
Final Report, May 2000

Prepared by:

BWRVIP REPAIR COMMITTEE
OAKRIDGE NATIONAL LABS
AUBURN UNIVERSITY
LOUISIANA STATE UNIVERSITY

Prepared for

BOILING WATER REACTOR VESSEL & INTERNALS PROJECT and
ELECTRIC POWER RESEARCH INSTITUTE

3412 Hillview Ave.
Palo Alto, California 94304

DISCLAIMER OF WARRANTIES AND LIMITATION OF LIABILITIES

This report was prepared by the organization(s) named below as an account of work sponsored or cosponsored by the BWR Vessel and Internals Project (BWRVIP) and the Electric Power Research Institute, Inc. (EPRI). Neither BWRVIP, EPRI, any member of EPRI, any cosponsor, the organization(s) named below, nor any person acting on behalf of any of them:

(a) makes any warranty or representation whatsoever, express or implied, (i) with respect to the use of any information, apparatus, method, process or similar item disclosed in this report, including merchantability and fitness for a particular purpose, or (ii) that such use does not infringe on or interfere with privately owned rights, including any party's intellectual property, or (iii) that this report is suitable to any particular user's circumstance, or

(b) assumes any responsibility for any damages or other liability whatsoever (including any consequential damages, even if BWRVIP, EPRI or any EPRI representative has been advised of the possibility of such damages) resulting from your selection or use of this report or any information, apparatus, method, process or similar item disclosed in this report.

Organization(s) that prepared this report:

**Oakridge National Labs
Louisiana State University
Auburn University
BWRVIP Repair Committee**

ORDERING INFORMATION

Requests for copies of this report should be directed to the BWRVIP Program Manager, 3412 Hillview Ave., Palo Alto, Ca. 94304, (415) 855-2340.

Table of Contents

Executive Summary	ix
1.0 Introduction and Summary Conclusions	1
2.0 Literature Survey	7
3.0 Flux Modeling.....	9
4.0 Calculations of Helium Production	13
5.0 Weldability Maps	15
Appendix A: Detailed Results of Literature Survey	A-1
Appendix B: Details of Flux Calculations.....	B-1

List of Tables

Table 1-1	Boron concentration in commercial alloys used in research and in a U.S. nuclear power plant.	16
Table 2-1:	Summary of investigations relevant to the repair welding of irradiated materials.....	18

List of Figures

Figure 1-1	Helium Generation from Boron and Nickel	22
Figure 3-1	Layout of the upper section of representative BWR-4 plant, R-Z plane	23
Figure 3-2	Layout of the lower section of representative BWR-4 plant, R-Z plane.	24
Figure 3-3	Segment of the representative BWR/4 (Horizontal plane through core center.)	25
Figure 3-4	Plot of fast neutron flux ($E > 1$ Mev) in the R-Z plane for the upper reactor internals.	26
Figure 3-5	Plot of thermal neutron flux ($E < 0.4$ eV) in the R-Z plane for the upper reactor internals.	27
Figure 3-6	Plot of fast neutron flux ($E > 1$ Mev) in a horizontal plane through the reactor vessel at the height of peak flux.	28
Figure 3-7	Plot of thermal neutron flux ($E < 0.4$ eV) in a horizontal plane through the reactor vessel at the height of peak flux.	29
Figure 3-8	Plot of fast neutron flux ($E > 1$ MeV) in the R-Z plane for the lower reactor internals.	30
Figure 3-9	Plot of thermal neutron flux ($E < 0.4$ MeV) in the R-Z plane for the lower reactor internals.	31
Figure 4-1	Concentration of helium generated from boron and from nickel.	32
Figure 5-1	Atomic ppm helium from 1 wt. ppm boron after one full power year for the upper half of the reactor.	33

Figure 5-2	Atomic ppm helium from 1 wt. ppm boron after 15 full power years for the upper half of the reactor.	34
Figure 5-3	Atomic ppm helium from 1 wt. ppm boron after 30 full power years for the upper half of the reactor.	35
Figure 5-4	Atomic ppm helium from 1 wt. ppm boron after 1 full power year for the lower half of the reactor.	36
Figure 5-5	Atomic ppm helium from 1 wt. ppm boron after 15 full power years for the lower half of reactor.	37
Figure 5-6	Atomic ppm helium from 1 wt. ppm boron after 30 full power years for the lower half of the reactor.	38
Figure 5-7	Atomic ppm helium generated from nickel in an alloy containing 10% nickel for the upper half of the reactor in one full power year.	39
Figure 5-8	Atomic ppm helium from nickel in an alloy containing 10% nickel for the upper half of the reactor in 15 full power years.	40
Figure 5-9	Atomic ppm helium from nickel in an alloy containing 10% nickel for the upper half of the reactor in 30 full power years.	41
Figure 5-10	Atomic ppm helium from nickel in an alloy containing 10% nickel for the lower half of the reactor in one full power year.	42
Figure 5-11	Atomic ppm helium from nickel in an alloy containing 10% nickel for the lower half of the reactor in 15 full power years.	43
Figure 5-12	Atomic ppm helium from nickel in an alloy containing 10% nickel for the lower half of the reactor in 30 full power years.	44

Executive Summary

The Boiling Water Reactor Vessel and Internals Project (BWRVIP) Repair Committee has been developing a welded repair option for Reactor Pressure Vessel (RPV) internal components. This repair option may be necessary for some components and configurations that are not suited to a mechanical repair, or where replacement requires structural welding.

Previous experience in welding components from high fluence regions indicates that cracking can occur due to the presence of helium, produced by transmutation, in the base metal.

This report provides a summary of available data on the effects of helium on weld repairs and provides a methodology for defining the components, in a typical BWR, that can currently be repaired by welding without encountering degraded weld quality due to the presence of helium.

1.0 Introduction and Summary Conclusions

In recent years, Boiling Water Reactors (BWRs) in the United States and Overseas have experienced stress corrosion cracking in a number of internal components. Significant cracking has occurred at such locations as jet pump riser pipes, core spray piping and core shrouds. In some cases the preferred, or only, method of repairing or replacing the affected component requires welding. For components located in regions of low neutron fluence, welding is relatively straightforward although requiring significant effort for developing automated welding equipment and qualification of procedures. In high fluence regions, however, welding is complicated by the deleterious effects caused by the presence of helium in the base metal. The helium is produced in the metal primarily by transmutation of boron and nickel. When the metal is liquefied during welding, the helium is released and causes porosity and cracking. Under high helium concentrations, the helium causes porosity along grain boundaries in the fusion zone. At lower concentrations, cracking occurs in the heat affected zone (HAZ) resulting from bubbles formed by migration of helium under the influence of high temperatures and stress.

In recognition of this problem, the Repair Committee of the Boiling Water Reactor Vessel and Internals Project (BWRVIP) initiated a study to better understand the implications of helium production on weld repairs. The primary objective of the work was to define which components in a typical BWR could be repaired by welding without showing degraded weld performance due to the presence of helium and which components would require additional work to confirm weldability or do not appear to be weldable. This objective was accomplished with a three-part approach:

1. Perform a literature search to determine maximum amount of helium that can exist in the base metal before weldability becomes impaired.
2. Perform analyses to determine the amount of helium which would be expected to exist in components located at various locations in a typical BWR. This was a two-step process which involved first calculating the neutron flux at each location and using these results to estimate the resulting helium concentration.
3. Developing a "weldability" map showing which locations in the reactor could be welded without exhibiting the deleterious effects due to helium.

The results of the literature search show that:

Content Deleted - EPRI Proprietary Information

The literature search is described in Section 2 of this report; the neutron flux and helium concentrations are discussed in Sections 3 and 4; and the weldability maps are shown in Section 5. In all cases, details of the various discussions are contained in Appendices. Some introductory technical details on the sources of helium in metals and the effect on weldability are discussed in the following paragraphs

Background

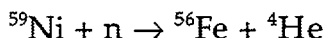
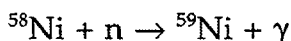
Helium is produced by irradiation of metals in what are known as (n,α) reactions. In this reaction, a nucleus in a metal absorbs a neutron and emits an alpha particle (which is identical to a helium nucleus). The helium atom thus produced is very stable and remains in the metal essentially forever. For high energy neutrons (above about 10 MeV) this reaction can occur with a large number of elements. However, for the thermal neutrons which occur in BWRs, those with energies less than approximately 0.5 eV, only a few elements undergo a significant number of (n, α) reactions. The most prominent elements are boron and nickel.

Boron is present in stainless steels and nickel base alloys in concentrations from below 5 wt. ppm to 30 wt. ppm or higher. It is simply a naturally occurring impurity. Table 1-1 lists the boron contents of a number of structural alloys taken from literature and some measurements of archive materials from an operating BWR. Boron has two naturally occurring isotopes ^{11}B and ^{10}B , the latter of which comprises 19.9% of boron. Only ^{10}B undergoes the (n,α) reaction with thermal neutrons, and its thermal cross section is very high (3840 barns). Because of the high cross section, it burns rather quickly, over 90% being burned to ^4He and ^7Li by a thermal fluence of 10^{21} n/cm^2 .

Since helium is such a light atom, it is often presented in atomic percent rather than weight per cent to give a better feel for the amount present. One

weight percent boron in iron is equivalent to 5.18 atomic percent. However, natural boron is only 19.9% ^{10}B , so one weight percent boron is equivalent to 1.03 atomic percent ^{10}B . We will consider this equal to one. Since every atom of ^{10}B will ultimately burn to ^4He , one weight percent natural boron will ultimately form one atomic percent helium. This is a convenient rule of thumb that will be used later.

Nickel becomes the larger source of helium at fluences beyond 10^{21} to 10^{22} n/cm^2 , depending upon the alloy. Its behavior is more complicated than that of boron in that a two step reaction is necessary. Nickel-58 comprises 68.1% of natural nickel and undergoes the following reactions with thermal neutrons:



Since ^{59}Ni is not naturally occurring, the production rate of helium is initially zero and increases as ^{59}Ni accumulates. Unlike boron, there is a more than adequate supply of nickel in any stainless steel or nickel alloy so that the concentration of helium grows to many thousands of atomic ppm given sufficient thermal fluence. Figure 1-1 shows helium production from both boron and nickel in stainless steel containing 10 wt. ppm boron as a function of thermal neutron fluence. For type 304 stainless steel, the cross over point where helium from nickel becomes greater than that from boron is at a thermal fluence of on the order of 7×10^{21} n/cm^2 .

A third source of helium is important to the study of welding in irradiated materials, although not an important source of helium in commercial BWR's. The method, known as the "tritium trick method", makes use of the fact that tritium, an isotope of hydrogen, decays to ^3He . This source of helium can be used to study the effects of helium on materials and, in particular, on welding. Tritium is diffused into the metal at elevated temperatures. For refractory metals, pressures below atmospheric are used, but for steels high pressures are required because of the lower solubility of hydrogen in iron. The metal is then cooled and aged at cryogenic temperatures until the desired concentration of helium is formed. It is then heated in a vacuum to permit the tritium to diffuse out, leaving the helium. The 12.3 year tritium half-life makes helium doping a slow process, but by using a sufficient amount of tritium, significant helium generation rates can be achieved. An advantage of the technique is that the material need not be neutron irradiated so that it is not activated. This eliminates the need for radiation hot cells for handling. However, since there is always residual tritium, a proper facility for containment of small amounts of tritium must be used.

Once helium is produced in sufficient quantities, it can cause serious defects in a welding process due to the fact that it is insoluble in metals. Helium diffuses through the metal lattice and segregates at defects and grain boundaries in the form of bubbles which destroy cohesion at grain boundaries and eventually cause failure. When the material is welded, helium bubbles are formed and, at sufficiently high concentrations, can be trapped in the fusion zone. At lower concentrations, damage occurs in the HAZ. Here the rapid diffusion associated with the high temperature allows rapid accumulation of helium in bubbles at grain boundaries. The presence of a tensile stress upon cooling is even more damaging since it makes larger bubbles thermodynamically more favorable. Rapid growth of the bubbles fed by rapidly diffusing helium leads to grain boundary cracking in the HAZ.

Evidence suggests that there is a threshold of helium concentration above which weldability becomes problematic. The literature search described in the following section was undertaken to attempt to establish that threshold.

2.0 Literature Survey of Repair Welding

A computer literature search was performed to determine the maximum amount of entrained helium which can be tolerated before adverse effects on weldability would be expected. The search was conducted on the following databases: Weldasearch, 1967; Metadex, 1966; Engineered Materials Abstracts, 1986; Energy Science and Technology, 1974; and Chemical Abstracts, 1967. The key word used to perform the search were: weld, irradiation, helium, steels, cracks and repair. The databases cover literature from 1966 to the present and include articles in all languages.

A total of over 300 scientific articles was identified from which a careful manual screening narrowed the number of relevant articles to 49. These 49 articles report the findings of 8 investigations that directly address the repair welding of irradiated materials. A detailed description of the results of the literature search is given in Appendix A. A summary of the findings of the 8 relevant investigations is shown in Table 2-1. The following conclusions can be drawn from the open literature:

**Content Deleted -
EPRI Proprietary Information**

**Content Deleted -
EPRI Proprietary Information**

3.0 Flux Modeling

From the preceding sections, it is evident that we need to determine the locations in a reactor at which the accumulated helium concentration is less than approximately 1 appm. The first step in calculating helium concentration is to calculate the thermal neutron flux. Once flux is known as a function of energy and position in the reactor, the reaction rate with boron and nickel can be calculated as a function of position. From this, the time dependent accumulation of helium can be calculated and, from that, the weldability assessed.

An accurate estimation of thermal flux in a specific BWR requires detailed calculations using plant specific input data. However, in order to provide an estimate of helium production, calculations were performed to determine the flux at all points in a typical reactor. A BWR-4 was chosen as the type of plant to be modeled because of its predominance in the fleet.

Content Deleted -

EPRI Proprietary Information

Details of the calculations performed are described in Appendix B. A summary of the methods used and the pertinent results are presented in the remainder of this section.

Description of the Flux Calculations

A complete three dimensional calculation of the flux everywhere within the reactor would be impractical. However, satisfactory results can be obtained by the "synthesis method" in which three separate calculations are performed and then synthesized into a three dimensional picture of the flux. A two dimensional calculation is done in the RZ plane and a similar calculation in the R Θ plane. A third one dimensional transport calculation is required in the radial direction. The three flux distributions are then combined according to the following equation, the parameters of which are rigorously defined in Appendix B:

$$\Phi(R, \Theta, Z) = \frac{\phi_{R, \Theta}(R, \Theta) \times \phi_{R, Z}(R, Z)}{\phi_R(R)}$$

where $\phi_{R, \Theta}$ = "R Θ channel" flux, obtained from a 2D transport calculation in R Θ geometry;

$\phi_{R, Z}$ = "RZ channel" flux, obtained from a 2D transport calculation in RZ geometry;

ϕ_R = "R channel" flux, obtained from a 1D transport calculation in R geometry, corresponding to a radial traverse along the core midplane in the RZ model.

This synthesis approach is commonly used for reactor flux calculations and is the approach recommended in NRC Draft Reg Guide DG-1053 (June 1996). It is the preferred method for determining pressure vessel fluences. The DORT transport code was used with a 47 group cross section library, SAILOR95.

Content Deleted -

EPRI Proprietary Information

The upper and lower regions were treated separately since the core midplane, which was chosen as the origin of the coordinate system, can be treated as a reflecting boundary. The R- theta model is shown in Figure 3-3. All components were modeled with known positions and average compositional number densities within each region.

Content Deleted -

EPRI Proprietary Information

It is important to realize that, although state of the art methods were used in the calculations and that fast fluxes are predicted rather well in cases where measurements have been made, thermal flux is difficult to predict. The homogenized nodes used in the calculations do not reflect the sometimes large local variations in thermal flux arising from the wide variations in thermal neutron cross sections between materials. Even in the small and relatively simple cores of research reactors, fast flux is predicted well, but unanticipated variations in thermal flux always exist, as indicated by flux monitors.

Results of Flux Calculations

Results of the calculations are shown in Figures 3-4 through 3-9. Figures 3-4 and 3-5 show the R-Z dependence of the fast and thermal flux in the upper core region. The various internal components are indicated by solid lines and can be identified by reference back to Figure 3-1.

Content Deleted -

EPRI Proprietary Information

Figure 3-6 and 3-7 show the azimuthal (Θ) variation of the flux at the location of peak axial fast and thermal flux (87.3 cm above the core midplane).

**Content Deleted -
EPRI Proprietary Information**

Figures 3-8 and 3-9 show the axial variation in fast and thermal flux respectively for the lower core region.

**Content Deleted -
EPRI Proprietary Information**

In using the figures to estimate the thermal flux at a particular location, the following guideline is suggested.

**Content Deleted -
EPRI Proprietary Information**

4.0 Calculations of Helium Production

The production of helium (appm) is shown in Figure 4-1 as a function of thermal fluence. The curve for helium from boron is for an alloy containing 1 wt. ppm boron. The curve for helium from nickel is for an alloy containing 10 percent nickel. To estimate the helium concentration in a metal sample located at a particular location in a reactor, the following procedure may be used:

**Content Deleted -
EPRI Proprietary Information**

For convenience, the equations of the curves on Figure 4-1 are presented below.

For the production of helium from boron:

**Content Deleted -
EPRI Proprietary Information**

and, for the production of helium from nickel:

**Content Deleted -
EPRI Proprietary Information**

For most situation in BWR locations of interest, the helium produced from boron (steps 1-4) will give a sufficiently accurate estimate of the helium

concentration. However, for high fluence regions the contribution to the helium concentration from the transmutation of nickel (steps 5-7) must also be considered.

**Content Deleted -
EPRI Proprietary Information**

5.0 Weldability Maps

Analyses were made to calculate helium concentrations throughout the typical reactor for in-service lifetimes of 1, 15 and 30 years. Figures 5-1 through 5-6 show helium concentrations from boron for a material containing 1 ppm boron; figures 5-7 to 5-12 are similar contour plots for helium produced from nickel in a material containing 10 percent nickel. The regions of weldability may be quickly determined using these figures by multiplying the results for boron by the boron concentration in the material and the nickel results by the ratio of the nickel concentration to 10 percent and adding the results for boron and nickel. For time periods not close to those in the graphs, the seven-step process described in Section 4 can be used. In using these results, it should be remembered that the fluence calculations were for a "typical" reactor and that plant specific fluences may differ somewhat.

**Content Deleted -
EPRI Proprietary Information**

Tables

Table 1-1 Boron concentrations in commercial alloys used in research and in a U.S. nuclear power plant

**Content Deleted -
EPRI Proprietary Information**

**Content Deleted -
EPRI Proprietary Information**

TABLE 2-1: Summary of Investigations Relevant to the Repair Welding of Irradiated Materials

**Content Deleted -
EPRI Proprietary Information**

TABLE 2-1 (con't): Summary of Investigations Relevant to the Repair Welding of Irradiated Materials

**Content Deleted -
EPRI Proprietary Information**

Figures

**Content Deleted -
EPRI Proprietary Information**

Fig. 1-1 Helium generation from boron and nickel. (A typical AISI type 304 stainless steel with 10% nickel and 10 wt. ppm boron is assumed.)

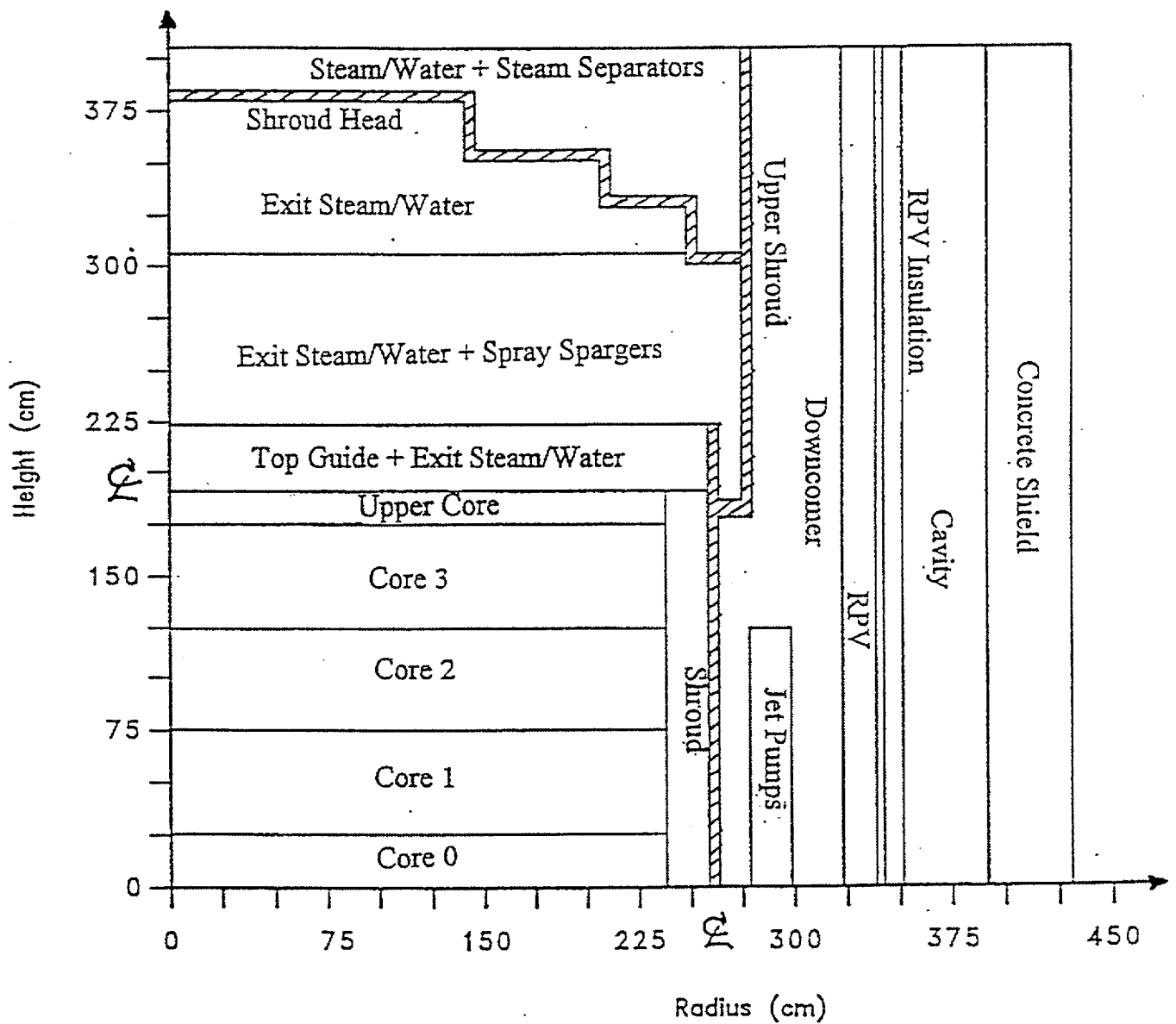


Fig. 3-1 Layout of the upper section of representative BWR-4 plant, R-Z plane (Origin of Z coordinate is the core midplane)

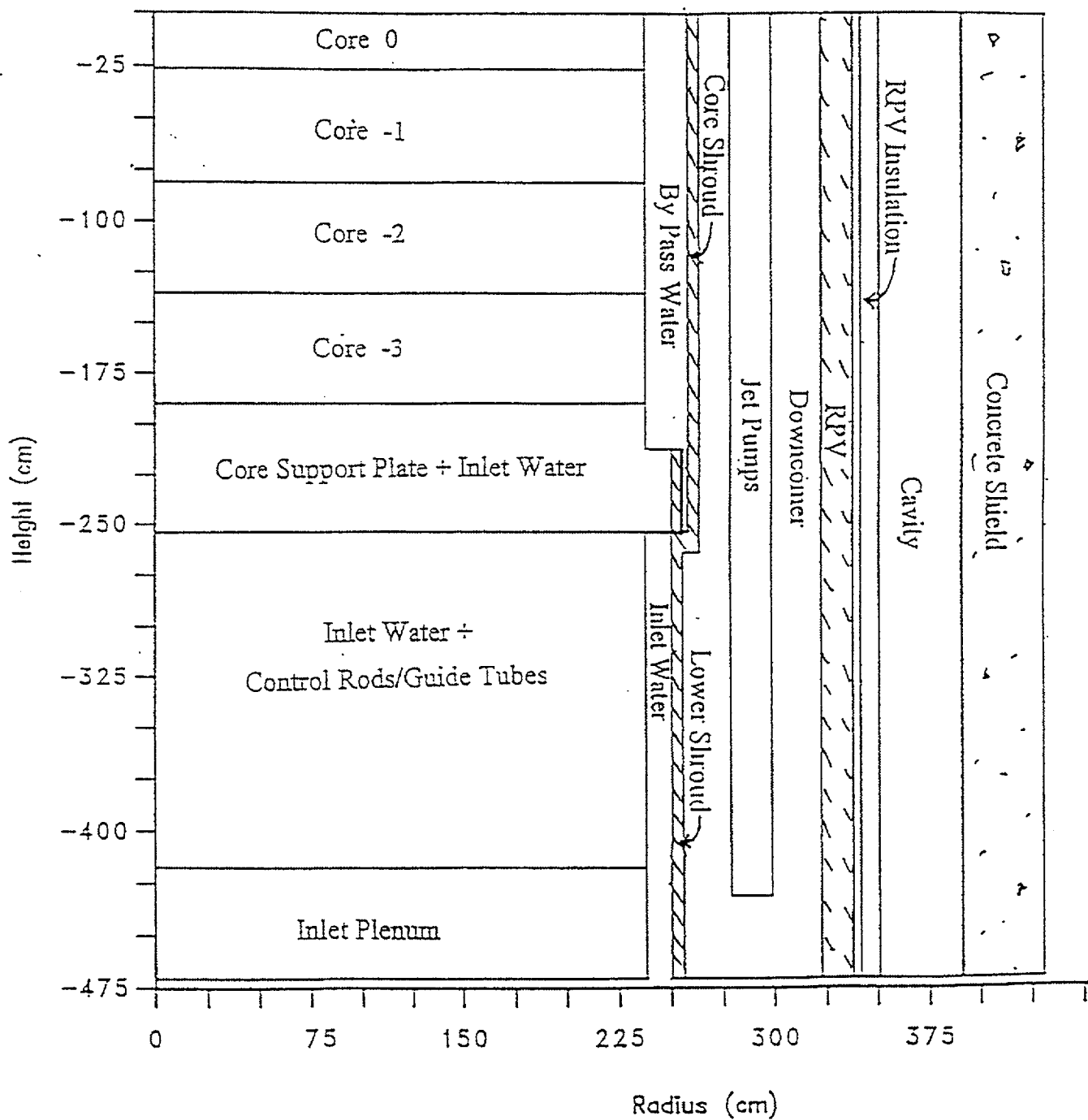
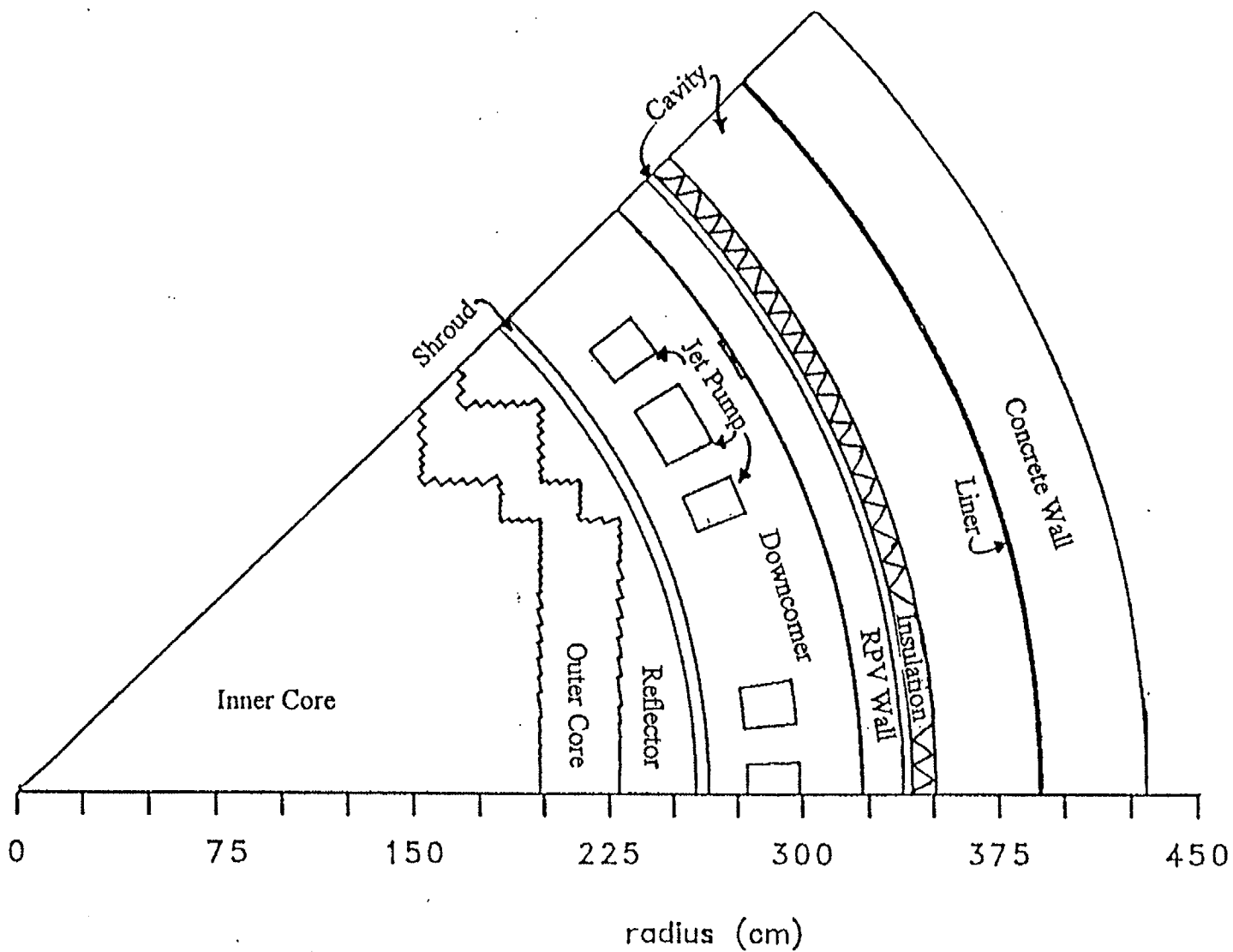


Fig. 3-2 Layout of the lower section of representative BWR/4 plant, R-Z plane. (Origin of the Z coordinate is the core midplane.)

Fig. 3-3 Segment of the representative BWR/4 (Horizontal plane through core center.)



**Content Deleted -
EPRI Proprietary Information**

Fig. 3-4 Plot of fast neutron flux ($E > 1$ Mev) in the R-Z plane for the upper reactor internals. (Solid lines indicate structures labeled in Fig. 3-1.)

**Content Deleted -
EPRI Proprietary Information**

Fig. 3-5 Plot of thermal neutron flux ($E < 0.4$ eV) in the R-Z plane for the upper reactor internals. (Solid lines indicate structures labeled in Fig. 3-1.)

Fig. 3-6 Plot of fast neutron flux ($E > 1$ Mev) in a horizontal plane through the reactor vessel at the height of peak flux. (Solid lines indicate structures labeled in Fig. 3-3.)

**Content Deleted -
EPRI Proprietary Information**

Fig. 3-7 Plot of thermal neutron flux ($E < 0.4$ eV) in a horizontal plane through the reactor vessel at the height of peak flux. (Solid lines indicate structures labeled in Fig. 3-3.)

**Content Deleted -
EPRI Proprietary Information**

**Content Deleted -
EPRI Proprietary Information**

Fig. 3-8 Plot of fast neutron flux ($E > 1$ MeV) in the R-Z plane for the lower reactor internals. (Solid lines indicate structures labeled in Fig. 3-2.)

**Content Deleted -
EPRI Proprietary Information**

Fig. 3-9 Plot of thermal neutron flux ($E < 0.4$ MeV) in the R-Z plane for the lower reactor internals. (Solid lines indicate structures labeled in Fig. 3-2.)

**Content Deleted -
EPRI Proprietary Information**

Fig. 4-1 Concentration of helium generated from boron and from nickel.
The data points on the nickel curve were from transport calculations
at randomly chosen points in the reactor. The boron curve uses
an average thermal cross section.

**Content Deleted -
EPRI Proprietary Information**

Fig. 5-1 Atomic ppm helium from 1 wt. ppm boron after one full power year for the upper half of the reactor.

**Content Deleted -
EPRI Proprietary Information**

Fig. 5-2 Atomic ppm helium from 1 wt. ppm boron after 15 full power years for the upper half of the reactor.

**Content Deleted -
EPRI Proprietary Information**

Fig. 5-3 Atomic ppm helium from 1 wt. ppm boron after 30 full power years for the upper half of the reactor.

**Content Deleted -
EPRI Proprietary Information**

Fig. 5-4 Atomic ppm helium from 1 wt. ppm boron after 1 full power year for the lower half of the reactor.

**Content Deleted -
EPRI Proprietary Information**

Fig. 5-5 Atomic ppm helium from 1 wt. ppm boron after 15 full power years for the lower half of the reactor.

**Content Deleted -
EPRI Proprietary Information**

Fig. 5-6 Atomic ppm helium from 1 wt. ppm boron after 30 full power years for the lower half of the reactor.

**Content Deleted -
EPRI Proprietary Information**

Fig. 5-7 Atomic ppm helium generated from nickel in an alloy containing 10% nickel for the upper half of the reactor in one full power year.

**Content Deleted -
EPRI Proprietary Information**

Fig. 5-8 Atomic ppm helium from nickel in an alloy containing 10% nickel for the upper half of the reactor in 15 full power years.

**Content Deleted -
EPRI Proprietary Information**

Fig. 5-9 Atomic ppm helium from nickel in an alloy containing 10% nickel for the upper half of the reactor in 30 full power years.

**Content Deleted -
EPRI Proprietary Information**

Fig. 5-10 Atomic ppm helium from nickel in an alloy containing 10% nickel for the lower half of the reactor in one full power year.

**Content Deleted -
EPRI Proprietary Information**

Fig. 5-11 Atomic ppm helium from nickel in an alloy containing 10% nickel for the lower half of the reactor in 15 full power years.

**Content Deleted -
EPRI Proprietary Information**

Fig. 5-12 Atomic ppm helium from nickel in an alloy containing 10% nickel for the lower half of the reactor in 30 full power years.

Appendix A

A LITERATURE REVIEW

OF

THE REPAIR WELDING OF IRRADIATED

STAINLESS STEEL MATERIALS

A-1: Computer Search Results

Five separate computer searches were conducted in September-October of 1996 using the WELDASEARCH, 1967-; METADEX, 1966-; ENGINEERED MATERIALS ABSTRACTS, 1986-; ENERGY SCIENCE AND TECHNOLOGY, 1974-; and the CHEMICAL ABSTRACTS, 1967-, databases to determine the information available in the literature related the weldability of irradiated materials. The key words used in the search include: weld, irradiation, helium, steels, crack, and repair. The individual data bases cover different initial periods of time to the present as indicated by the date following the database listing. The earliest database that was searched covers literature from 1966 to the present. Searches included articles published in all languages. A total of over 300 scientific articles were identified which met the key word requirements. A careful manual screening of these abstracts narrowed the number of relevant articles to 49 that address the repair of irradiated materials. All the other articles are devoted to welding of unirradiated materials for reactor applications. Publication information on articles relevant to the weld repair of irradiated structures are given in Table A-1.

A-2: Summary of Relevant Investigations:

**Content Deleted -
EPRI Proprietary Information**

**Content Deleted -
EPRI Proprietary Information**

**Content Deleted -
EPRI Proprietary Information**

**Content Deleted -
EPRI Proprietary Information**

**Content Deleted -
EPRI Proprietary Information**

**Content Deleted -
EPRI Proprietary Information**

**Content Deleted -
EPRI Proprietary Information**

**Content Deleted -
EPRI Proprietary Information**

**Content Deleted -
EPRI Proprietary Information**

**Content Deleted -
EPRI Proprietary Information**

**Content Deleted -
EPRI Proprietary Information**

**Content Deleted -
EPRI Proprietary Information**

**Content Deleted -
EPRI Proprietary Information**

**Content Deleted -
EPRI Proprietary Information**

**Content Deleted -
EPRI Proprietary Information**

A-3. Summary

This report addresses the welding of structural materials containing helium. Helium is produced during neutron irradiation of materials through two basic mechanisms: nuclear reactions with the alloying elements and impurities present in the materials and diffusion of tritium into the metal followed by subsequent decay of the tritium to helium. In the case of light water reactors, helium results from transmutation of boron and at fluences above 10^{25} n/m², nickel.

**Content Deleted -
EPRI Proprietary Information**

Table A-1: Literature Relevant to Repair Welding of Irradiated Materials

**Content Deleted -
EPRI Proprietary Information**

Table A-1 (cont): Literature Relevant to Repair Welding of Irradiated Materials

**Content Deleted -
EPRI Proprietary Information**

Table A-1 (cont): Literature Relevant to Repair Welding of Irradiated Materials

**Content Deleted -
EPRI Proprietary Information**

Table A-1 (cont): Literature Relevant to Repair Welding of Irradiated Materials

**Content Deleted -
EPRI Proprietary Information**

Table A-1 (cont): Literature Relevant to Repair Welding of Irradiated Materials

**Content Deleted -
EPRI Proprietary Information**

Table A-1 (cont): Literature Relevant to Repair Welding of Irradiated Materials

**Content Deleted -
EPRI Proprietary Information**

Table A-1 (cont): Literature Relevant to Repair Welding of Irradiated Materials

**Content Deleted -
EPRI Proprietary Information**

Table A-1 (cont): Literature Relevant to Repair Welding of Irradiated Materials

**Content Deleted -
EPRI Proprietary Information**

Appendix B

Thermal Neutron Flux Calculations

TRANSPORT CALCULATIONS OF NEUTRON EXPOSURE TO IN-VESSEL COMPONENTS **Deleted**

M. L. Williams , M. Asgari
January, 1997

I. DESCRIPTION OF CALCULATION METHOD

Neutron transport calculations were performed to determine the thermal flux ($<0.4\text{eV}$), the helium production rate via $^{10}\text{B}(n,\alpha)$ reactions, and the flux above 1 MeV within the internal structural components of the **Deleted** boiling water reactor. Of particular interest are the flux and reaction rates within: (a) structural components above the active core height ("upper internals"), (b) structural components below the active core height ("lower internals"), (c) the lower, middle, and upper shroud, and (d) inlet piping entering the shroud about 1-2 feet above the active core, which carries water to core spray spargers. The desired quantities were computed by "synthesizing" fluxes obtained from 2 two dimensional transport calculations --in R θ and RZ cylindrical geometries, respectively-- along with a single 1D radial calculation. These three sets of results can be combined in the manner described in reference 1 to obtain an approximate 3D distribution in R θ Z coordinates, given by:

$$\Phi(R,\theta,Z) = \frac{\phi_{R,\theta}(R,\theta) \times \phi_{R,Z}(R,Z)}{\phi_R(R)} \quad (1)$$

where $\phi_{R,\theta}$ = "R θ channel" flux, obtained from a 2D transport calculation in R θ geometry;
 $\phi_{R,Z}$ = "RZ channel" flux, obtained from a 2D transport calculation in RZ geometry;
 ϕ_R = "R channel" flux, obtained from a 1D transport calculation in R geometry,
 corresponding to a radial traverse along the core midplane in the RZ model;

Equation 1 is essentially a type of single-channel synthesis approximation. The channel fluxes were calculated with the discrete ordinates transport code DORT⁽²⁾, using the new 47 group cross section library called "SAILOR95"⁽³⁾. SAILOR95 is an updated and much improved version of the original SAILOR⁽⁴⁾ library widely used in pressure vessel fluence calculations. The cross sections in SAILOR95 are based on similar data as in BUGLE-93⁽⁵⁾, except the self-shielding and materials compositions in the former library is tailored to LWR applications. Some of the major improvements in the multigroup nuclear data contained in SAILOR95 compared to SAILOR are:

- (a) Cross sections are processed from ENDF/B-VI rather than the older ENDF/B-IV data. Changes in the iron inelastic cross sections in version VI significantly improve the computation of neutron transport through steel.
- (b) An improved approach for self-shielding cross sections of structural materials is utilized in producing the SAILOR95 group data.
- (c) Four thermal groups are used in SAILOR95 to account for upscattering in the energy

range below 1.86 eV, while no upscatter reactions are included in the original SAILOR thermal data.

Item (c) especially has a major impact on computation of thermal flux and reaction rates. It has been found that calculations of thermal parameters with the *original* SAILOR data are essentially unreliable. However initial testing of SAILOR95 indicate that it is able to closely reproduce the thermal flux computed by a fine-group library that has many more thermal groups⁽³⁾. In order to properly utilize the multiple thermal group data in SAILOR95 it is necessary to perform "outer iterations" in the transport calculations. DORT converges thermal fluxes very slowly, and many outer iterations are required to obtain the desired thermal responses, requiring several days of CPU time for some DORT runs on a SUN SPARC-20 Workstation. No previous studies have attempted to determine the thermal flux in the ex-core region of a LWR using such a detailed computational approach as utilized in this work.

The synthesis approach used in this study to obtain 3D fluxes is recommended in the NRC draft Reg Guide DG-1053 (June 1996)⁽⁶⁾ as the preferred method for determining pressure vessel fluence, and it has been benchmarked in numerous experiments that established its accuracy for calculations of the fast flux near the reactor midplane elevation. However only minimal testing of the synthesis method has been performed for thermal reaction rates and for axial locations above or below the active core. To the authors' knowledge, no fast or thermal dosimetry measurements have ever been performed for these regions. One of the main uncertainties in the synthesized flux calculated for regions above and below the active core height is the question of what is the appropriate azimuthal distribution.

II. REACTOR MODELS USED IN TRANSPORT CALCULATIONS.

In order to obtain the $R\theta$ and RZ fluxes used in the synthesis method, it is necessary to perform two dimensional (2D) calculations in two types of 2D cylindrical coordinate systems. An $R\theta$ coordinate system corresponds to a slice through an infinitely tall cylinder, in which the neutron source and material composition (and hence the flux) can vary azimuthally (θ) and radially (R). The irregularly shaped core boundary must be represented by different radii, as a function of theta. This causes the ex-core flux to vary significantly as a function of θ for a fixed radius, since the amount of water between the core boundary and the shroud radius changes as θ changes. Figure 1 shows the **Deleted** BWR as modeled in $R\theta$ geometry for the transport calculations. In the present work the $R\theta$ calculation provides the azimuthal shape of the ex-core flux for elevations within the active core height; and it was also optionally used for approximating the azimuthal variation of the flux above or below the active core. The DOTSOR⁽⁷⁾ program obtained the neutron source for the DORT transport calculations by transforming the core power distribution into a corresponding source density distribution defined on the appropriate $R\theta$ mesh. The cycle-averaged, assembly power distribution used in these calculations was computed from cycle burnup data provided by **Deleted** based on their 3D nodal calculation performed with SIMULATE. The assembly powers are shown in figure 2

Content Deleted -

EPRI Proprietary Information

that the power shape within the boundary assemblies can affect the computed fluxes in ex-core

It is known

components such as the shroud and pressure vessel; therefore it was necessary to compute an approximate "intra-assembly" power shape for the outer bundles. This was done using a one-dimensional cylindrical model of the **Deleted** core-reflector-shroud-downcomer regions. An eigenvalue calculation with the discrete ordinates code XSDRNPM⁽⁹⁾ determined the space dependent fission source near the core boundary. No variation in enrichment or burnable poison concentration within the outer bundles is treated in this simple 1D model. The radial power shape was found to peak at the edge of the core, and also at the water gap on the inner-side of the peripheral bundle, as shown in figure 3. This radial distribution was used to represent the intra-assembly power shape for all peripheral bundles in the DORT 2D models; the intra-assembly power shape was assumed to be flat for all interior bundles.

A complication encountered in BWR calculations is the question of what composition to use for the core region in the R θ model. While the composition of a PWR core is essentially uniform axially, the void fraction changes significantly at different elevations in a BWR. The amount of leakage from the core is affected by the density of water (viz, hydrogen) in the core. A void fraction of about 50% was used in the R θ model, which corresponds roughly to the midplane void fraction. Note that the impact of the *axial variation* in the void fraction is accounted for in the RZ transport calculation, as discussed below.

Figures 4 and 5 show the RZ models of the upper and lower axial regions, respectively, used in the DORT calculations. The 1D radial model (R) is defined by a radial traverse of either RZ model at the core midplane ($Z=0$), either including or not including, respectively, the homogenized jet pumps in the model [both approaches were utilized]. In order to reduce the size of the problem, only one half of the reactor is modeled in each RZ calculation, with a reflected boundary condition along the reactor midplane. Although the axial power distribution is not exactly symmetrical, we have established that the flux in region above and below the active core, respectively, is not sensitive to the power beyond the midplane, so that a reflected boundary at the midplane causes essentially no error in the calculations. The origin of the Z axis used in the RZ transport calculations is located at the center of the active core; hence elevations above the reactor midplane have positive Z coordinates, while those below the midplane have negative Z values. The dimensions and compositions for the two RZ models were obtained from **Deleted** plant engineering drawings. The plant drawings are relative to a zero elevation at the bottom inside of the vessel, and indicate the elevation of the middle of the active fuel to be at an elevation of 291.3125", or 739.93 cm. Therefore *all Z coordinates shown in tables and figures in this report must be increased by 739.93 cm. to relate the position to a corresponding elevation in the plant drawings.*

Although two-dimensional RZ geometry is able to correctly represent the radial and axial variation in the reactor dimensions and compositions, it must assume that the components are *axi-symmetrical*. For true cylindrical components like the shroud, vessel, etc. this assumption is strictly correct; however, the outer boundary of the core region can not be exactly modeled in RZ geometry, since it is not axi-symmetrical (i.e., the core radius is a function of θ). In RZ geometry (and also in one dimensional R geometry) the core must be represented by some axi-symmetrical cylindrical volume with an "effective" radius. There is no single best method to select the effective radius. For the effective radius in our RZ and R models we have used an "average" radius which preserves the total core volume. It has been demonstrated in PWR analysis that

synthesized 3D fluxes near the beltline region are not very sensitive to the outer core radius used in the RZ and R models, since these two fluxes appear as a *ratio* in eq. 1, but this has not been proven for axial locations outside of the active core height, nor for BWR's which have axially varying compositions. Regardless of how the effective radius is selected, the core source distribution in the RZ and R calculations are normalized to give the proper value for the volume integrated power, so that the total number of neutrons produced per second throughout the core is correct.

The axial source distribution for the RZ model was determined from the SIMULATE burnup distribution provided by **Del**. It was observed from the SIMULATE results that all interior assemblies have similar axial power shapes; however, the axial variation of the power in the outer bundles is somewhat different. Thus a different axial source distribution was used for the outermost 6 inches of the core region in the DORT RZ model to represent the axial shape in the peripheral assemblies. Figure 6 shows the two axial power shapes used in the RZ calculations. The radial shape of the source near the core boundary was the same as described for the "intra-assembly" power shape of peripheral bundles in the R θ model.

Material compositions in the various zones of the DORT models are homogenized mixtures of water, stainless steel, core, etc. based on volume fractions given in the plant engineering drawings. A typical axial void distribution was used to determine the core water density as a function of elevation in the active core: seven zones with different void fractions were represented in the DORT RZ models to account for the variation in the water density from the core inlet to the outlet. The core inlet water is slightly sub-cooled, while the exit void fraction at the top of the core is set to 70%. The water/steam mixture within the shroud dome above the core was assumed to be at 65% void; while water above the dome and outside the shroud was represented as saturated liquid. The upper guide plate and sparger ring are homogenized with water in the upper internal zones of the RZ model. The water below the core is sub-cooled at 1000 psi, and has a density of about 0.74 g/cc. Like the upper internals, the lower internals (eg, bottom support plate, control rod guide tubes, etc) also are represented by homogenized mixtures of steel and water. **Deleted** contains 185 cruciform control rods which have a length approximately equal to the active core height. After consultation with **Del**, it was decided to represent the control rod insertion pattern by 12 "deep rods" which are fully inserted; 12 "shallow rods" which are inserted up to an elevation of about 109 cm (43 inches) above the bottom of the core; and the remainder of the rods are assumed to be fully withdrawn, extending into the lower internals region below the core⁽¹⁰⁾. The B₄C absorber in the blades was uniformly homogenized within the volumes containing the control rods---no spatial self-shielding corrections were made in the homogenization process, so the rod worth will be somewhat over-estimated. The impact of uncertainties in the control representation is discussed in a later section. Table 1 lists the compositions of all materials used in the DORT transport models.

Both the R θ and RZ models include the ex-vessel reactor cavity and concrete shield regions. Axial streaming occurs in the cavity region between the vessel and the concrete shield, and this effect has been shown to increase the flux in the outer section of the RPV at elevations far above the midplane. However at radial positions located several inches inside of the vessel IR (such as near the shroud), the impact of cavity streaming should be negligible, due to the shielding provided by the downcomer; but this is not necessarily the case for downcomer locations adjacent

to the vessel. The angular quadrature used in the discrete ordinates calculations is an S8 order, which has 48 directions represented. A higher order quadrature may be required in the RZ calculation to accurately compute the axial transport of neutrons in the cavity, at elevations significantly above or below the midplane.

III. AZIMUTHAL SHAPE OF THE FLUX

The three dimensional group fluxes in this work are obtained from the single-channel synthesis expression given in eq. 1. This expression can also be written as

$$\Phi(R, \Theta, Z) = \phi_{R, \Theta}(R, \Theta) \times L_Z(R, Z) \quad (2)$$

where

$$L_Z(R, Z) = \frac{\phi_{R, Z}(R, Z)}{\phi_R(R)} \quad (3)$$

In eq. 2 the R Θ -channel flux $\phi_{R, \Theta}$ is considered the primary flux variable, and L_Z is a factor that accounts for the axial variation, which is approximated as being independent of Θ . Use of an azimuthally-independent axial factor has been shown to be a very good approximation over the height of the active core. In fact in RPV fluence studies, where the beltline fluence is of primary concern, the axial factor can often be obtained directly from the axial shape of the core power without even requiring RZ and R transport calculations⁽⁶⁾.

The azimuthal variation in the synthesized flux computed with eq. 2 is determined entirely by the azimuthal shape of the R Θ channel flux, $\phi_{R, \Theta}$. Within the elevation of the active core height the azimuthal variation in the ex-core flux is very significant, because the water thickness between the core outer boundary and the shroud is a function of theta, and because boundary assemblies at different azimuths may produce different amounts of power. At radii beyond the shroud in a BWR, the jet pumps also introduce an additional azimuthal dependence. There are typically several maxima and minima in the azimuthal shape of the flux: the flux usually peaks at azimuths of least distance between the core and shroud, or at azimuths where hot assemblies are loaded on the core boundary. There may be up to a factor of 6-7 difference between the maximum and minimum ex-core flux as a function of Θ , for a fixed radius at the beltline in the shroud or vessel. The synthesis method has been previously benchmarked for the fast flux at elevations within the active core height; however in computing the fluence received by the upper and lower internals outside of the core height it is necessary to extend the synthesis method beyond its usual range of application, so that some consideration must given to the best way of utilizing the approximation.

Another equivalent way of expressing the synthesized flux in eq. 1 is,

$$\Phi(R, \Theta, Z) = \phi_{R, Z}(R, Z) \times A_{\Theta}(R, \Theta) \quad (4)$$

where the "azimuthal variation function" has been defined as,

$$A_{\theta}(R, \theta) = \frac{\phi_{R,\theta}(R, \theta)}{\phi_R(R)} \quad (5)$$

Now the RZ channel flux is viewed as the primary variable, and $A_{\theta}(R, \theta)$ gives the relative azimuthal shape at all Z coordinates. The single-channel synthesis method does not allow the azimuthal shape to change at different elevations. While this approximation is reasonable within the height of the active core, it is questionable at elevations significantly above or below the active core region where the azimuthal shape of the flux is not well known. It is expected physically that the relative azimuthal variation slightly above or below the top or bottom of the active fuel, respectively, should be similar to that within the active height; but the peaks and valleys in the flux will eventually "smooth out" to a more uniform azimuthal shape at greater distances beyond the core. At this time the azimuthal shape within the "transitional range" of elevations is not well established either by experimental analysis or by true three dimensional calculations. Hence three possible options were considered for representing the azimuthal shape of the flux:

- (a) The channel flux $\phi_{R\theta}$ for use in eq. 5 is computed from an R θ model of the midplane geometry, which includes the azimuthal variation in the core boundary and the jet pumps at their appropriate theta locations. This approximation could be used for elevations inside of the core within the height of the jet pumps.
- (b) The channel flux $\phi_{R\theta}$ for use in eq. 5 is computed from an R θ model of the midplane geometry, but the jet pumps are omitted in the R θ model. This approximation could be used above the elevation of the jet pumps, such as in the upper internals.
- (c) Finally, the azimuthal variation in the flux caused by the irregular core boundary could be assumed to be completely damped out above and below the core; thus the R θ distribution of the flux is uniform. This amounts to assuming that the factor A_{θ} in eq. 5 is unity, so that the *RZ calculation alone* provides the flux distribution a function of radius and height, but no θ variation is included. This approximation is a possible alternative to methods (a) and (b) at "sufficiently" removed elevations from the core.

The "correct" azimuthal distribution at any particular elevation is unknown, but presumably can be approximated as some combination of these three solutions. In order to provide an estimation for the sensitivity of calculated values to this modelling approximation inherent in the synthesis approach, results were computed using both methods (a) and (c) at the location of the core spray inlet pipe above the T.A.F. (top of active fuel), and using methods (b) and (c) at the elevation of the shroud support, below the B.A.F. (bottom of active fuel). These results are discussed in sections VI and VII.

IV. PERTURBATION IN B^{10} REACTION RATE DUE TO PIPE WALLS

At a given location, the thermal flux may be impacted by the presence of localized components, such as pipes, spargers, steam separators, etc. These types of geometrical irregularities can not be modelled in the DORT 2D coordinate systems, so it is necessary to homogenize the components in the transport calculations. In order to determine the thermal reaction rate within the walls of a steel component such as a pipe, a heterogeneous correction must be made to correct for the effect of the pipe on the local thermal flux. Of particular interest

in the present study is the rate of helium production by ^{10}B reactions in the coolant pipe that supplies water to the core spargers located above the active core. The inlet pipe is oriented radially across the downcomer, and enters the upper shroud about 1-2 feet above the active core. It is not possible to explicitly represent a pipe with this orientation in either the R θ or RZ cylindrical coordinate systems described in section II; therefore the results synthesized from the 2D models do not account for the perturbation in the flux caused by the presence of the pipe itself. The 0.3 inch walls of the stainless steel pipe tend to reduce the thermal flux and boron reactions due to the higher thermal absorption cross section of steel compared to water, and even more due to the displacement of the water moderator. Hence, additional one-dimensional transport calculations were performed to assess the effect of the stainless steel pipe omitted from the primary 2D models used to compute the unperturbed results at the sparger inlet location.

A 1D model of the pipe in both cylindrical and slab geometries, respectively, was used to compute a "perturbation factor" to correct the boron reaction rate computed from the synthesized fluxes. Both types of geometries were found to give similar results. The transport model consists of three zones corresponding to, respectively, the water inside of the pipe, the steel wall of the pipe, and an exterior water region about 1 cm thick outside of the pipe. The flux spectrum on the outer boundary of the exterior region is assumed to be unperturbed by the pipe walls. A boundary source with an energy spectrum obtained from the 2D RZ run at the approximate radial and axial location of pipe was used to represent the unperturbed spectrum that exists away from the influence of the pipe. The perturbation factor is computed from the ratio of the B10 reaction rates with and without the steel pipe wall represented in the transport calculations; i.e., with either steel or water, respectively, included at the location of the pipe walls. Results are shown below.

**Content Deleted -
EPRI Proprietary Information**

V. RESULTS OF CALCULATIONS FOR REACTOR BELTLINE REGION

At elevations near the reactor beltline the standard synthesis expression in eq.2 can be used to compute the group fluxes. The 47 group fluxes found in the transport calculations are used to obtain the thermal flux, the boron reaction rate, and the fast flux, respectively.

**Content Deleted -
EPRI Proprietary Information**

**Content Deleted -
EPRI Proprietary Information**

VI. RESULTS OF CALCULATIONS FOR UPPER INTERNALS

Figures 12-14 show iso-contours for these three responses *based only on the RZ transport calculations* from the core midplane throughout the upper internals above the core. The flux from the RZ calculation alone with no azimuthal factor approximates the value of the flux *averaged over θ* , as a function of radius and elevation

**Content Deleted -
EPRI Proprietary Information**

**Content Deleted -
EPRI Proprietary Information**

VI-a. Sensitivity of Results in Upper Internals to Modeling Approximations in RZ Model

As discussed in previous sections, approximations must be made in the transport calculations that determine the absolute flux spectrum in the region of interest. We have attempted to use best estimates (rather than strictly conservative values) for various input and modelling parameters, so that the results represent the "most likely" values. In order to obtain an indication of the sensitivity of the computed results to some of the modelling parameters used in the 2D RZ transport calculations, a series of one-dimensional axial calculations was performed for the core and upper internals. In these transport calculations, various input parameters were changed, and the resulting change in the boron reaction (ie, helium production rate) along the centerline was observed. The one-dimensional model for all cases is a slab corresponding to an axial traverse from the core mid-plane to the water region above the shroud head dome. The specific 1D cases considered in the sensitivity study are summarized below.

**Content Deleted -
EPRI Proprietary Information**

**Content Deleted -
EPRI Proprietary Information**

VII. RESULTS OF CALCULATIONS FOR LOWER INTERNALS

The lower internals region located below the core contains the bottom support plate, and the guide tubes for control rods and instrumentation. The flux at the shroud and bottom support of the jet pumps is also of interest. The flux in the lower internals is much less than that in the upper internals due to two factors: (a) the inlet water is sub-cooled liquid instead of 65% voided water, like the core exit coolant, and (b) the withdrawn control rods that extend below the core absorb many of the thermal neutrons.

Figures 17-19 show iso-contours for the three responses *based only on the RZ transport calculations* from the core midplane throughout the lower internals region. Recall that the flux from the RZ calculation alone with no azimuthal factor approximates the value of the flux averaged over Θ , as a function of radius and elevation.

**Content Deleted -
EPRI Proprietary Information**

VII-a. Sensitivity of Thermal Flux in the Lower Internals to Control Rod Representation

The flux below the core is impacted by the fully and partially withdrawn control rods that extend below the active core height. It is necessary to make several simplifying approximations to represent the absorber material in these rods in the DORT RZ calculations.

**Content Deleted -
EPRI Proprietary Information**

VIII. ESTIMATED UNCERTAINTY IN CALCULATIONS

Much of the work in this study has not been validated by experimental measurements or by more rigorous computational methods such as Monte Carlo; hence the uncertainty in the computed values is very difficult to quantify. A rough estimate for uncertainties based on the major contributors is given below. *These values are strictly "estimates".*

**Content Deleted -
EPRI Proprietary Information**

REFERENCES

1. P. Chowdhury, M. L. Williams, F. B. K. Kam, "Development of a Three-Dimensional Flux Synthesis Program and Comparison with 3D Transport Theory Results", ORNL/TM-10503 (NUREG/CR-4984), Oak Ridge National Laboratory, January, 1988.
2. "TORT-DORT Two- and Three-Dimensional Discrete Ordinates Transport Version 2.8.14", RSIC Computer Code Collection CCC-543, available from the Radiation Shielding Information Center, Oak Ridge National Laboratory, PO Box 2008, Oak Ridge, TN 37831-6362.
3. M. L. Williams, M. Asgari, H. Manohara, "Letter Report on Generating SAILOR95 Library", Louisiana State University communication sent to F. B. K. Kam and J. V. Pace at Oak Ridge National Laboratory, February, 1995.
4. G. L. Simmons, R. W. Roussin, "SAILOR: Coupled, Self-Shielded, 47 Neutron, 20 Gamma Ray, P3, Cross Section Library for Light Water Reactors", RSIC-DLC-76, Oak Ridge National Laboratory, June 1980.
5. "BUGLE-93, Production and Testing of the VITAMIN-B6 Fine-Group and the BUGLE-93 Broad Group Neutron/Photon Cross Section Libraries Derived from ENDF/B_VI Nuclear Data," RSIC-DLC-175, Oak Ridge National Laboratory, February 1994.
6. "Calculational and DOSIMETRY Methods for Determining Pressure Vessel Neutron Fluence". DRAFT REGULATORY GUIDE DG-1053, U. S. Nuclear Regulatory Commission, Office of Nuclear Regulatory Research, June 1996.
7. M. L. Williams, "DOTSOR: A Module in the LEPRICON Computer Code System for Representing the Neutron Source Distribution in LWR Cores", EPRI Interim Report [available from the Radiation Shielding Information Center, Oak Ridge National Laboratory, PO Box 2008, Oak Ridge, TN 37831-6362], Electric Power Research Institute, December 1985.
8. Letter to M. L. Williams from Ken Knoll, Pennsylvania Power & Light, CCN 741070, FILE A7-8B, PLE-19751, Nov. 1, 1996.
9. L. M. Petrie, N. M. Greene, "XSDRNPM-S: A One-Dimensional Discrete Ordinates Code For Transport Analysis", U. S. Nuclear Regulatory Commission, NUREG/CR-0200, Vol.2, Sec. F3 of *SCALE System Documentation*, Oak Ridge National Laboratory, 1982.
10. Personal Communication to M. L. Williams, via phone conversation with Paul Lee, Pennsylvania Power & Light, November 15, 1996.

TABLE 1. Material Compositions used in DORT Calculations

**Content Deleted -
EPRI Proprietary Information**

**Content Deleted -
EPRI Proprietary Information**

**Content Deleted -
EPRI Proprietary Information**

**TABLE 2. AZIMUTHAL VARIATION AT SHROUD INNER RADIUS ($R=258$ cm.),
AT PEAK-FLUX ELEVATION**

**Content Deleted -
EPRI Proprietary Information**

**TABLE 3. AXIAL VARIATION AT SHROUD I. R., AND AT AZIMUTH OF MAXIMUM
THERMAL FLUX (R = 258 cm.)**

**Content Deleted -
EPRI Proprietary Information**

**TABLE 3. AXIAL VARIATION AT SHROUD I. R., AND AT AZIMUTH OF MAXIMUM
THERMAL FLUX, *continued***

**Content Deleted -
EPRI Proprietary Information**

**TABLE 4. RADIAL VARIATION THROUGH THE CENTER OF THE JET PUMP AT
30.3 °, AT ELEVATION OF PEAK FLUX**

**Content Deleted -
EPRI Proprietary Information**

**TABLE 5. AXIAL VARIATION ALONG REACTOR CENTERLINE:
FROM T. A. F. (@190.5 cm.) THROUGH UPPER INTERNALS**

**Content Deleted -
EPRI Proprietary Information**

**TABLE 5. AXIAL VARIATION ALONG REACTOR CENTERLINE: CORE MIDPLANE
THROUGH UPPER INTERNALS, *continued***

**Content Deleted -
EPRI Proprietary Information**

**TABLE 6. RADIAL VARIATION AT ELEVATION OF T.A.F, AND AT
AZIMUTH OF MAXIMUM SHROUD-FLUX**

**Content Deleted -
EPRI Proprietary Information**

**TABLE 6. RADIAL VARIATION AT ELEVATION OF T.A.F., AND AT
AZIMUTH OF MAXIMUM SHROUD-FLUX, *continued***

**Content Deleted -
EPRI Proprietary Information**

**TABLE 6. RADIAL VARIATION AT ELEVATION OF T.A.F., AND AT
AZIMUTH OF MAXIMUM SHROUD-FLUX, *continued***

**Content Deleted -
EPRI Proprietary Information**

TABLE 7. SYNTHESIZED RESULTS AT SPARGER INLET PIPE, USING R θ CALCULATION WITH NO JET PUMPS INCLUDED ⁽¹⁾

**Content Deleted -
EPRI Proprietary Information**

**TABLE 8. RESULTS AT SPARGER INLET PIPE ,USING FLAT AZIMUTHAL SHAPE
(i.e., No Synthesis; Based only on RZ calculation with effective core radius⁽¹⁾)**

**Content Deleted -
EPRI Proprietary Information**

**TABLE 9. AXIAL VARIATION ALONG REACTOR CENTERLINE THROUGH
LOWER INTERNALS**

**Content Deleted -
EPRI Proprietary Information**

**TABLE 9. AXIAL VARIATION ALONG REACTOR CENTERLINE THROUGH
LOWER INTERNALS, *continued***

**Content Deleted -
EPRI Proprietary Information**

**TABLE 9. AXIAL VARIATION ALONG REACTOR CENTERLINE THROUGH
LOWER INTERNALS, *continued***

**Content Deleted -
EPRI Proprietary Information**

***TABLE 10. RADIAL VARIATION AT TOP OF CORE BOTTOM SUPPORT PLATE, AND
AT AZIMUTH OF MAXIMUM SHROUD-FLUX***

**Content Deleted -
EPRI Proprietary Information**

**TABLE 10. RADIAL VARIATION AT TOP OF CORE BOTTOM SUPPORT PLATE, AND
AT AZIMUTH OF MAXIMUM SHROUD-FLUX, *continued***

**Content Deleted -
EPRI Proprietary Information**

**TABLE 10. RADIAL VARIATION AT TOP OF CORE BOTTOM SUPPORT PLATE, AND
AT AZIMUTH OF MAXIMUM SHROUD-FLUX, *continued***

**Content Deleted -
EPRI Proprietary Information**

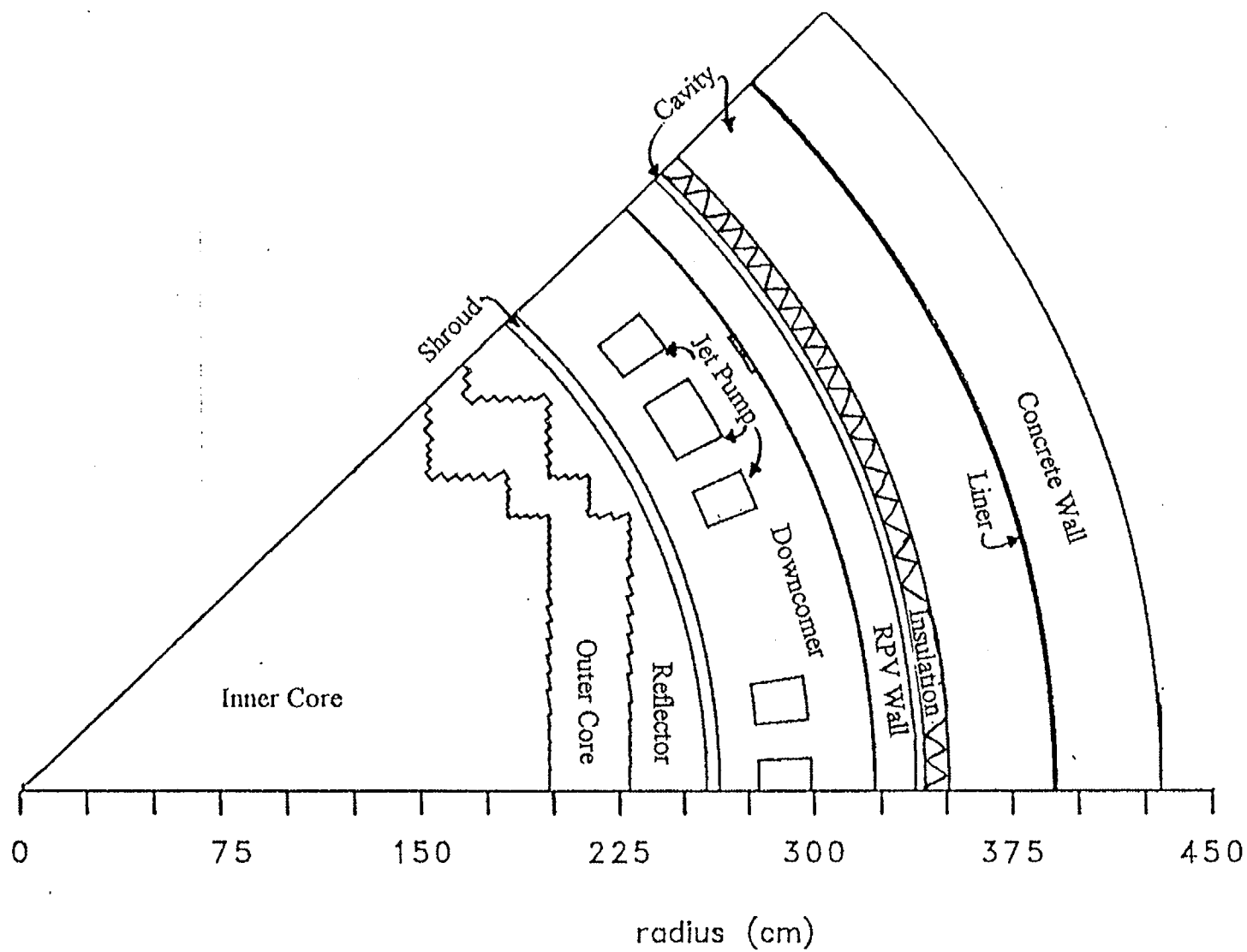
**TABLE 11. SYNTHESIZED RESULTS AT TOP OF LOWER SHROUD SUPPORT,
USING AZIMUTHAL VARIATION BASED $R\theta$ CALCULATION WITH
JET PUMPS INCLUDED⁽¹⁾**

**Content Deleted -
EPRI Proprietary Information**

**TABLE 12. RESULTS AT TOP OF LOWER SHROUD SUPPORT, USING FLAT
AZIMUTHAL SHAPE (i.e., No Synthesis; Based only on RZ calculation with
effective core radius)**

**Content Deleted -
EPRI Proprietary Information**

FIGURE 1. R-Theta Geometry Plot



**Content Deleted -
EPRI Proprietary Information**

Figure-3. Relative Radial Power Distribution Within a Peripheral Assembly

**Content Deleted -
EPRI Proprietary Information**

FIGURE 4. R-Z Geometry for Upper Internals

**Content Deleted -
EPRI Proprietary Information**

FIGURE 5. R-Z Geometry for Lower Internals

**Content Deleted -
EPRI Proprietary Information**

Figure-6. Relative Axial Power Distribution

**Content Deleted -
EPRI Proprietary Information**

**Figure-7. R θ Isoplot of Absolute Synthesized Fast Flux ($E > 1.0$ MeV)
at Peak Axial**

**Content Deleted -
EPRI Proprietary Information**

Figure-8. $R\theta$ Isoplot of Absolute Synthesized Thermal Flux ($E < 0.4$ eV)
at Peak Axial

**Content Deleted -
EPRI Proprietary Information**

Figure-9. R θ Isoplot of Absolute Synthesized B-10(n, α) reaction Rate
Per Atom (*1.0E24) at Peak Axial

**Content Deleted -
EPRI Proprietary Information**

Figure-10. Radial Variation of Absolute Neutron Flux at Azimuthal and Axial Peak Location

**Content Deleted -
EPRI Proprietary Information**

Figure-11. Radial Variation of Boron-10(n,alpha) Reaction Rate Per Atom Through Core Shroud(R=258-263) at Azimuthal and Axial Peak Location

**Content Deleted -
EPRI Proprietary Information**

Figure-12. RZ Isoplot of Fast Flux ($E > 1.0$ MeV) For Upper Internals

**Content Deleted -
EPRI Proprietary Information**

Figure-13. RZ Isoplot of Thermal Flux ($E < 0.4$ eV) For Upper Internals

**Content Deleted -
EPRI Proprietary Information**

Figure-14. RZ Isoplot of B-10(n,alpha) reaction Rate Per Atom (*1.0E24) For
Upper Internals

**Content Deleted -
EPRI Proprietary Information**

**Figure-15. Radial Variation Through Upper Core Shroud and Downcomer at the Elevation of Sparger Inlet
Pipe(~42 cm above T.A.F.)**

**Content Deleted -
EPRI Proprietary Information**

Figure-16. Axial Variation, Above Top of Active Core Elevation (H=190.5 cm), Flux at Mid-Downcomer (R=300.0 cm)

**Content Deleted -
EPRI Proprietary Information**

Figure-17. RZ Isoplot of Fast Flux ($E > 1.0$ MeV) For Lower Internals

**Content Deleted -
EPRI Proprietary Information**

Figure-18. RZ Isoplot of Thermal Flux ($E < 0.4$ eV) For Lower Internals

**Content Deleted -
EPRI Proprietary Information**

Figure-19. RZ Isoplot of B-10(n,alpha) reaction Rate Per Atom (*1.0E24) For
Lower Internals

**Content Deleted -
EPRI Proprietary Information**

Target:


Nuclear Power

About EPRI

EPRI creates science and technology solutions for the global energy and energy services industry. U.S. electric utilities established the Electric Power Research Institute in 1973 as a nonprofit research consortium for the benefit of utility members, their customers, and society. Now known simply as EPRI, the company provides a wide range of innovative products and services to more than 1000 energy-related organizations in 40 countries. EPRI's multidisciplinary team of scientists and engineers draws on a worldwide network of technical and business expertise to help solve today's toughest energy and environmental problems.

EPRI. Powering Progress

© 2000 Electric Power Research Institute (EPRI), Inc. All rights reserved. Electric Power Research Institute and EPRI are registered service marks of the Electric Power Research Institute, Inc. EPRI. POWERING PROGRESS is a service mark of the Electric Power Research Institute, Inc.

 Printed on recycled paper in the United States of America

TR-108707NP